Wetting and interfacial chemistry of metallic films on the hydroxylated α-$Al_2O_3(0001)$ surface

Rémi Lazzari[1,2,*] and Jacques Jupille[1,2,†]

[1]*Laboratoire CNRS/Saint-Gobain "Surface du Verre et Interfaces", 39 Quai Lucien Lefranc, BP 135, 93303 Aubervilliers, France*

[2]*Groupe de Physique des Solides, CNRS UMR 7588-Universités Paris 6 et 7, Campus Boucicaut, 140 Rue de Lourmel, 75015 Paris, France*

(Received 25 May 2004; revised manuscript received 6 October 2004; published 11 January 2005)

The wetting and the interfacial chemistry of titanium, aluminium, and silver films on hydroxylated α-$Al_2O_3(0001)$ surface have been studied *in situ* during the growth of the films. The wetting was probed by surface differential reflectance and the chemistry by photoemission. On the bare α-$Al_2O_3(0001)$, the examination of the O 1*s* level shows that the (1×1)-unreconstructed surface cannot be completely dehydroxylated, even by annealing in vacuum, the fingerprint of the remaining OH ($3\pm1.5\times10^{14}$ OH cm^{-2}) being a high binding energy O 1*s* shift. The first atomic layer of either titanium or aluminium reacts with the surface OH to produce an oxidized layer of atomic thickness. The metallic films then grow in a 3D mode on this intermediate oxidized layer, so that cleavage is expected to occur at the Me-Me/Me-O-Al interface (Me=Al, Ti). Therefore, hydroxylation does not appear as a panacea to promote perfect wetting for metals on alumina. The Ag/Ti/alumina assembly has also been examined. Contrasted behaviors are observed depending on whether titanium is in the oxide (0.2 nm) or in the metallic form (>0.2 nm). In the former case, wetting by silver shows little difference with respect to bare alumina, while silver wets almost perfectly the alumina covered by metallic titanium.

DOI: 10.1103/PhysRevB.71.045409 PACS number(s): 68.55.Ac, 68.08.Bc, 78.20.−e, 79.60.−i

I. INTRODUCTION

The interface chemistry is stressed to be a key ingredient in the adhesion between metals and oxides. Indeed, the nature of the metal-oxide (M-O) bond and the respective contributions of the long- and short-range interactions are still debated, in particular because the interfacial oxide is often not formed.[1] The molecular orbital picture of Johnson and Pepper[1] was first to stress the mostly covalent character of the short-range contribution to the M-O bond. The interaction between the metal *d* orbitals and the nonbonding oxygen *p* orbitals results in metal(*d*)-oxygen(*p*) bonding and antibonding molecular orbitals. Its strength decreases from early transition metals to noble metals as the *d*-band occupancy increases[2–4] so that the M-O adhesion correlates with the affinity of the metal for oxygen.[5] (A noticeable ionic character is also predicted for strong M-O bonds such as those involving isolated adatoms,[6] early transition metals[7] or *sp* metals.[8]) In turn, the weak adhesion energy of late transition metals and noble metals on oxides is mainly due to long range forces, i.e., image[6,9] and van der Waals.[10,11] The M-O adhesion energy W_{adh} is governed by the balance between the surface energy of the metal (γ_M) and of the oxide (γ_O), and by the interface energy ($\gamma_{M/O}$, which is the energy to be spent to create a unit area of M-O interface), as expressed by the Young-Dupré equation,

$$W_{adh} = \gamma_M + \gamma_O - \gamma_{M/O},$$

or by the Young-Dupre formula:

$$W_{adh} = \gamma_M(1 + \cos\theta),$$

where θ is the M-O contact angle. For noble metals on insulating oxides, θ is higher than 90° ($W_{adh} < \gamma_M$), while for transition metals and simple metals it lies around or slightly below 90° ($W_{adh} > \gamma_M$).[5,12] Small differences in contact angle may result in contrasted behaviors, from a poor wetting ($\theta > 90°$) to a quick percolation ($\theta < 90°$). Generally speaking, metals do not perfectly wet insulating oxides[2] and the search to improve M-O adhesion is a constant concern.

It is in this context that the chemistry of the surface OH groups of the oxide with the metal adlayer has been examined, in particular in the α-$Al_2O_3(0001)$ case.[13–17] Widely used as support for catalysts, thermal and corrosion barriers, possible substitute to silica in microelectronic devices, alumina is among the most common ceramics. Indeed, its wetting by metals is predicted to strongly depend on its surface termination.[8,18–20] Expected to be poor on the Al-terminated surface that is the equilibrium profile in oxygen-deficient environment, it should be stronger on the O-terminated surface. For example, the high adhesion energy of niobium on alumina is stressed to arise from the reversal of the stability of the surface leading to a Nb-O-Al interface via a niobium-aluminium exchange.[7] Therefore, the capability of α-$Al_2O_3(0001)$ to easily hydroxylate by dissociative adsorption of water[21–24] appears crucial since the hydroxylated surface can be viewed as a H-stabilized O-terminated α-$Al_2O_3(0001)$, which might open ways to grow strongly bound metal adlayers. Surface OH were claimed to enhance the adhesion energy at the Co/α-$Al_2O_3(0001)$ interface[17] through a Co-OH reaction. However, the suggestion that they improve the wetting of alumina by copper via an oxidation of the metallic $Cu^{(0)}$ into $Cu^{(1)}$ (Refs. 14 and 15) is questioned by Wang *et al.*[16] who predict instead a weakening of the Cu-alumina adhesion in the presence of OH. Similar concerns might apply to thick metal coatings on oxides. Due to dissipation, such coatings commonly show fracture toughness higher than 100 J m^{-2}, which is at least two orders of magnitude higher than the above-defined thermodynamic adhesion energy W_{adh}, but the exposure to moist air dramatically weakens the M-O toughness in a way that is not understood.[25]

 ©2005 The American Physical Society

While liquid/solid interfaces can be probed by the sessile drop method,[5,12] the analysis of solid-solid M-O thermodynamics is a challenging issue because techniques are lacking to characterize *in situ* the wetting behavior of a growing film. The hint of the present work is to analyze (i) the morphology of metallic films—and thus the wetting properties—during the growth of the films by surface differential reflectance (SDR)[26–29] (Sec. III) and (ii) to use in parallel photoelectron spectroscopy to characterize the charge transfer at the M-O interface (Sec. III A). Attention is focused herein on the chemistry at titanium and aluminium interfaces with hydroxylated α-$Al_2O_3(0001)$ in connection with the wetting properties of these interfaces. These systems have been chosen because their expected capability to dissociate surface OH of alumina (Ref. 16 for aluminium and comparison with cobalt in Ref. 17 for titanium) make them suitable to explore the metal-OH chemistry. Another way to gain insight into the electronic state of the very first metallic adlayers is the study of the wetting of an extra metal on the M-O system. This is the so-called buffer effect.[30,31] On α-$Al_2O_3(0001)$, predeposited buffer layers are quite effective in improving the adhesion of noble metals.[25,27,30–33] which were suggested to be glued by transition and *sp* metals through a depletion in the interfacial electronic density.[30,31] Silver was studied herein because it poorly wets alumina [contact angle 127°–131° (Refs. 5 and 12)] and undergoes little charge transfer at the interface,[6,34] so that the buffer effect should be clear (Sec. III C). It was first foreseen to examine the Ag wetting of both Ti- and Al-covered alumina. However, as shown below, the growth mode of Al/alumina is too far from two-dimensional (2D) to allow an additional Ag layer to be analyzed in good conditions. Therefore, the Ag wetting was only characterized on the Ti-covered alumina as a function of the Ti chemical state.

II. EXPERIMENT

Experiments were performed in an ultrahigh vacuum chamber with a base pressure in the low 10^{-8} Pa which was equipped with a low energy electron diffractometer (LEED) from Princeton Instruments and a x-ray photoemission spectrometer (XPS) VG Clam II with Al $K\alpha$ and Mg $K\alpha$ x-ray sources. Once inserted in the main chamber via a load-lock system, samples were stored on a carrousel. Sample holders could be screwed onto the end of a transfer bar with two degrees of freedom (translation and rotation), picked up from the carrousel and moved onto the different dedicated positions (gas dosing, deposition, low energy electron diffraction (LEED), XPS and surface differential reflectance (SDR), all instruments being mounted on translators to allow the bar to move). Annealing (up to 1200 K) and cooling (down to 180 K) of the sample, as well as temperature measurement by a chromel-alumel thermocouple were achieved via a device which was secured to the sample holder once it was screwed onto the transfer bar. The principle of that was to slip the sample holder within the device (in the same way as in the carrousel), which was transferred from a translator to the bar (and vice versa). The sample holder was a 25×30 mm^2 molybdenum piece with a hole opened in it (15×15 mm^2). The sample itself was clamped on a 10×10 mm^2 plate made of platinum to avoid the contamination of the sample via volatile oxides when exposed to oxygen at high temperature. The plate was in turn mounted through thin wires above the hole of the holder, so that the sample could be heated by an electron bombardment of the plate without heating too strongly the sample holder. The sample was cooled via a copper thread (long enough not to restrict the sample movement within the chamber) connected to a copper block cooled by circulating liquid nitrogen.

Gases were introduced via a leak valve through a dosing pipe made of a bunch of nickel tubes of diameter 1 mm (length 50 mm) inserted in a larger tube of diameter 7 mm. An equivalent pressure on the sample surface, estimated to 2 orders of magnitude higher than the stationary pressure (10^{-5} Pa), was achieved by setting the sample within a millimeter of the doser. High water pressure exposure were performed in the lock-load system of the chamber. Metallic fluxes were calibrated by a quartz microbalance (XTC, Leybold Infincon Ltd.). Al and Ag were evaporated from effusion cells carefully degassed before use, on the sample set upside down to allow SDR spectra to be recorded *in situ* during deposition. The pyrolytic boron nitride cell containing Al was degassed just above the melting point of the metal (930 K). It was annealed at 1270 K over several minutes before use to completely remove oxide from the metal in the cell.[35–37] Ti was evaporated from a tungsten wire wrapped with a Ti ribbon. It was checked by XPS that the deposited metals were free of impurity. The Ti thickness was calibrated from the O 1*s*(substrate)/Ti 2*p*(film), assuming a 2D Ti growth mode and using tabulated escape lengths ($\lambda_{\mathrm{O}\,1s}^{\mathrm{Al_2O_3}} = 16.8$ Å, $\lambda_{\mathrm{O}\,1s}^{\mathrm{Ti}} = 18.3$ Å, $\lambda_{\mathrm{Ti}\,2p}^{\mathrm{Ti}} = 18.3$ Å)[38,39] and ionization cross section [$\sigma(\mathrm{O}\,1s)/\sigma(\mathrm{C}\,1s) = 2.85$, $\sigma(\mathrm{Ti}\,2p_1/2)/\sigma(\mathrm{C}\,1s) = 2.68$, $\sigma(\mathrm{Ti}\,2p_3/2)/\sigma(\mathrm{C}\,1s) = 5.22$]. The results were in agreement with *ex situ* calibration via x-rays microprobe. The $10 \times 10 \times 1$ mm^3 alumina crystals were provided by Mateck GmBh.[40] After a short *ex situ* annealing at $T \sim 1300$ K for several hours, the AFM image showed ~ 200 nm wide terraces separated by steps of atomic height (Fig. 1). In the vacuum chamber, surfaces were cleaned at 1200 K by exposure to oxygen in front of the dosing pipe under an equivalent pressure close to 10^{-3} Pa. This temperature of 1200 K is below the lowest temperature at which the under-stoichiometric reconstruction occurs,[41] as demonstrated by the (1×1) LEED pattern with rather sharp spots that were recorded (Fig. 1). After a typical annealing of 10 to 20 minutes, the carbon coverage was below the detection limit of the XPS (~ 0.005 monolayer).

No charge compensation was provided on the insulating alumina during the photoemission measurements. Most XPS spectra have been collected at a take-off of $\Theta = 25°$ with respect to the surface normal. The Ti Auger parameter was obtained by adding the Ti $2p_{3/2}$ binding energy (BE) and the kinetic energy of the LMV Auger transition. The XPS peak analysis of Al 2*s*, O 1*s*, Ti 2*p* was performed after a subtraction of a Shirley background,[42] with either Gaussian-Lorentzian *s* peaks, *p* peaks (with the constraints of a $1/2$ ratio between the $1/2$ and $3/2$ components) or with a Doniach-Sunjic line shape in the case of Ti metal. The spin-

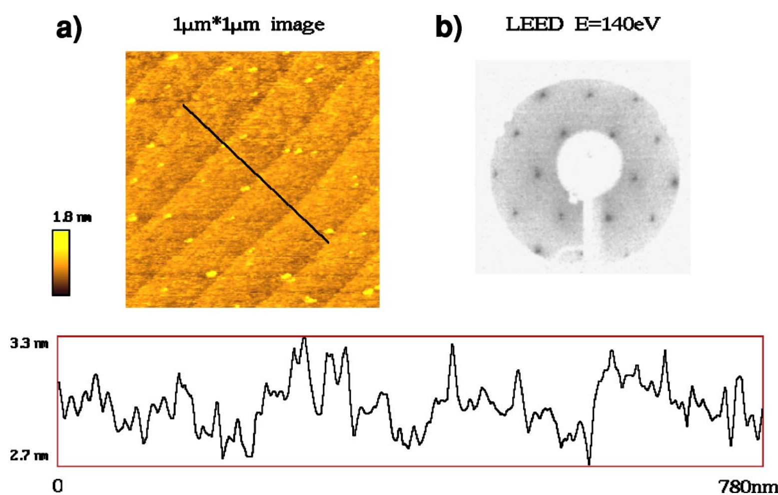

FIG. 1. (Color online) (a) 1×1 μm AFM image of a bare $Al_2O_3(0001)$ substrate after an *ex situ* annealing at 1270 K showing ~200 nm wide terraces. Also shown is the profile along the line shown in the figure. (b) (1×1) LEED pattern acquired on such surface after an *in situ* cleaning procedure.

orbit splitting was set to tabulated values for Ti^{4+} (5.8 eV), Ti^{2+} (5.9 eV), and Ti^0 (6.1 eV).

To record SDR spectra, two silica windows were installed on each side of the chamber. The surface of the sample could be illuminated at an incident angle of 45° through one of these by a deuterium lamp whose spectral range extended from the near infrared (1.5 eV or 820 nm) to the near ultraviolet (6 eV or 210 nm). The scattered light was polarized in the plane of incidence (*p* polarization) or perpendicular to it (*s* polarization) and then was collected through the other window via a condenser lens and an optical fiber to be analyzed by a grating spectrometer coupled with an array of 1024 silicon photodiodes connected to a computer. The principle of the analysis consisted in measuring in all the accessible spectral range, simultaneously, the relative change in reflectivity of the sample $\Delta R/R=(R-R_0)/R_0$, where R_0 is the reflectivity of the bare surface and R that of the metal-covered sample. The acquisition time, about a second, is two to three orders of magnitude lower than the deposition time. The spectra have been analyzed in the framework of the surface susceptibilities models developed by Bedeaux and Vlieger[43] in the quasistatic limit (under the assumption that the size of the particles is much smaller than the optical wavelength). The optical response during metal deposition is driven by the dielectric response of the growing nanoparticles, i.e., by their mean polarizabilities. The cluster shapes are assimilated to truncated spheres or spheroids whose polarizabilities are evaluated through a previously developed multipolar expansion of the potential.[28,29,44–47] As already demonstrated,[26,27,29] the high sensitivity of the spectra to the particle aspect ratio (i.e., its diameter seen from above divided by its height) can be used to probe the wetting of the metallic film. The dielectric constant of silver used herein[48] was finite size corrected.[45] The convergence of the simulation was ensured by including a sufficiently high number of multipoles ($M=16$ in general). To account for heterogeneous broadening of the resonances in the fit process, the calculated clusters polarizabilities have been folded by a Gaussian, thus keeping the integrated oscillator strength constant.

III. RESULTS AND DISCUSSION

A. Chemistry at the metal/alumina interface

Ti and Al films were deposited separately on oxygen annealed α-$Al_2O_3(0001)$ surfaces. The chemical state of the surface will be clarified later. Hydroxylated alumina can be prepared by exposure to water at pressure of the order of 1 torr (Ref. 49) and characterized by means of the O 1*s* core level shift. Surface OH groups manifest themselves by an O 1*s* shift which previous estimates were 1.5 ± 0.2 eV (Ref. 50) or 1.6 ± 0.2 eV,[51] close to measurements by other groups (1.3 eV[15] and 1.7 eV[17]). This shift was demonstrated to clearly differ from that due to molecular water[51] (2.9 ± 0.2 eV) and to be associated with a stretching OH mode at 3720 cm^{-1} in the high resolution energy loss spectrum (HREELS) of the alumina surface.[21,51] It corresponds to reversibly adsorbed OH. However, a component with a similar shift[14,15,51,52] is observed even after annealing the alumina surface in ultrahigh vacuum (see Fig. 1 in Ref. 50) at the highest temperature before reconstruction.[41] Depending on the thermal treatment, i.e., annealing in vacuum or under oxygen, this extra component amounts to 3–5% or 8–10% of area of the bulk O 1*s* peak. The assignment of this feature to irreversibly adsorbed OH is consistent with the observation of surface hydrogen by ion scattering.[53] However, it has never been directly evidenced. The goal of the present section is to examine the reaction between the deposited metal and the surface oxygen species and to identify these.

1. The one-atomic layer thick titanium oxide interlayer

Ti 2*p* and O 1*s* spectra recorded during the early stages of the growth of Ti/α-$Al_2O_3(0001)$ at 300 K are shown in Fig. 2. The Ti coverage is given in terms of average thickness. The strong change in the Ti 2*p* line shape in the early stage of the growth [Fig. 2(a)] is indicative of a Ti oxidation. Simultaneously, the higher BE O 1*s* (+1.5 eV) component of the clean surface undergoes a dramatic shift of -2.8 ± 0.2 eV, i.e., giving rise to a component shifted by -1.3 eV eV with respect to the bulk alumina O 1*s* [Fig. 2(b)] which has al-

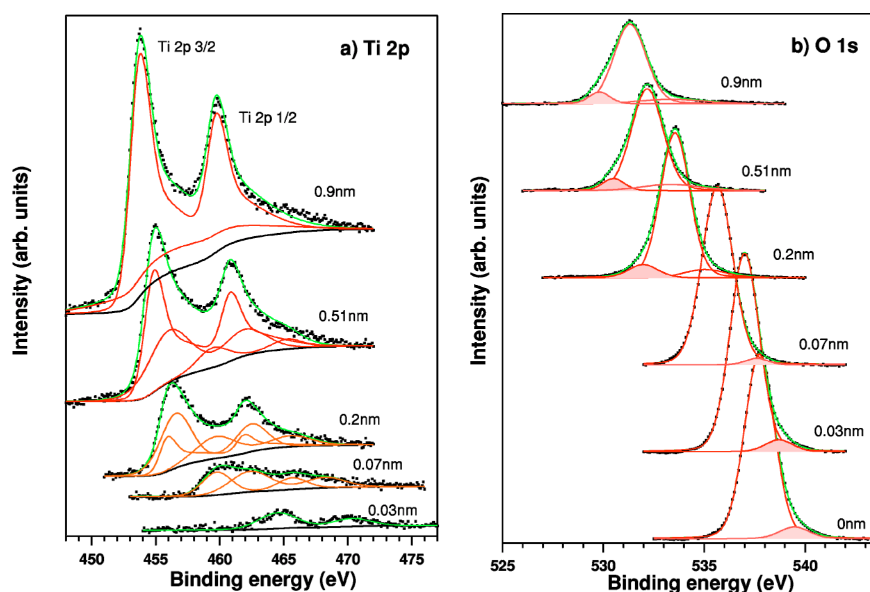

FIG. 2. (Color online) XPS spectra recorded during the deposition of titanium on α-$Al_2O_3(0001)$ at room temperature: (a) Ti 2p and (b) O 1s core levels and the associated peak decomposition (see text), with an emphasis on the early stage of the growth. The equivalent titanium thickness is given in the figure.

ready been observed in a previous study.[50] The −2.8 eV shift of that component as a whole on the O 1s lower BE side after a deposition slightly above a Ti monolayer (i) proves that it belongs to the very surface of alumina and (ii) suggests a chemical change from a given surface oxygen species to another. [Since titanium grows epitaxially with $(0001)Ti \parallel (0001)Al_2O_3$,[54,55] one Ti monolayer corresponds to a thickness of 0.186 nm.] It has been previously observed that Al 2s spectra do not show any shifted component upon Ti deposition.[50] However, the pending question[50] is the origin of the oxygen species corresponding to the residual +1.5 eV O 1s component that remains after annealing in vacuum [0 nm in Fig. 2(b)]. To solve the case, the behavior of the related oxygen species at the contact of metallic adlayer has been examined in details.

Prior to discussing the Ti-alumina reaction, references must be defined to determine absolute BE values. The thick Ti film (0.9 nm) is clearly metallic since the Ti 2p level at 453.8 ± 0.2 eV [Fig. 3(a)], the Auger parameter of 873.4 eV (Fig. 4) and the spin-orbit splitting of 6 eV closely compare the tabulated values of 454 ± 0.2 eV, 873.1 eV, and 6.1 eV (Ref. 56) and the values measured on a polycrystalline platinum foil (Fig. 4). In addition, as the metal Ti film grows, the Al 2s (Ref. 50) and O 1s (Fig. 2) levels show faint but real asymmetries on the higher BE side. Mimicked in the case of the O 1s spectra by a broad extra component [Fig. 2(b)], such an asymmetry could be partially assigned to the formation of electron-hole pairs via energy losses undergone by photoelectrons from the alumina substrate on their way through the metal Ti film. Therefore, the Ti 2p level associated to that Ti overlayer can serve as an internal reference, because the metallicity of the film prevents charging effect. However, another reference is required for the photoemission lines of the growing nonmetallic Ti layer. Assuming that the only lineup problem is at the Ti/alumina interface and that this lineup does not depend on the thickness of the film or, in

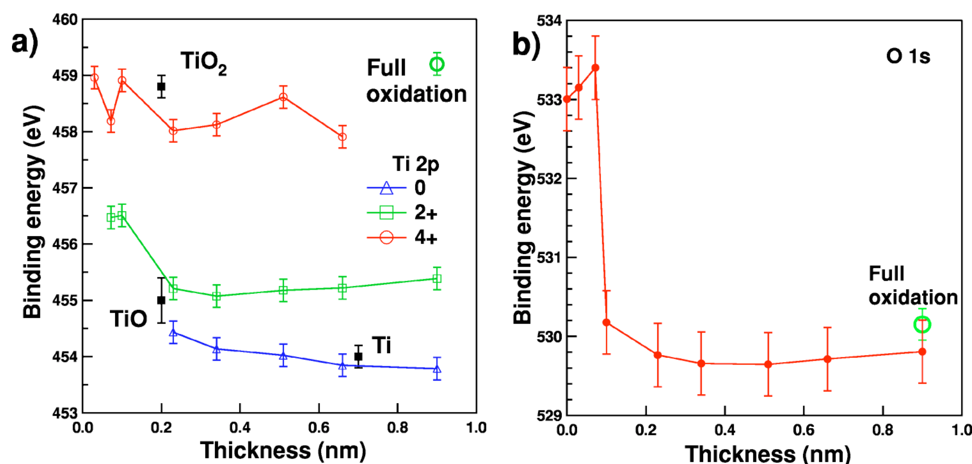

FIG. 3. (Color online) Deposition of titanium on alumina (thickness is indicated in figure): (a) Binding energy of the various components of the Ti 2p core level (labeled $Ti^{(0)}$, $Ti^{(2+)}$, $Ti^{(4+)}$—absolute values of the binding energy have been determined by taking the alumina core levels as references, see the text) and (b) the associated shift of the surface component of the O 1s core level. The bar on the left panel indicates the tabulated values of binding energy (from Ref. 56) for various titanium oxidation states. The circle on the two panels corresponds to the measured value after a full oxidation of the deposition under an oxygen partial pressure at high temperature ($T \sim 800$ K).

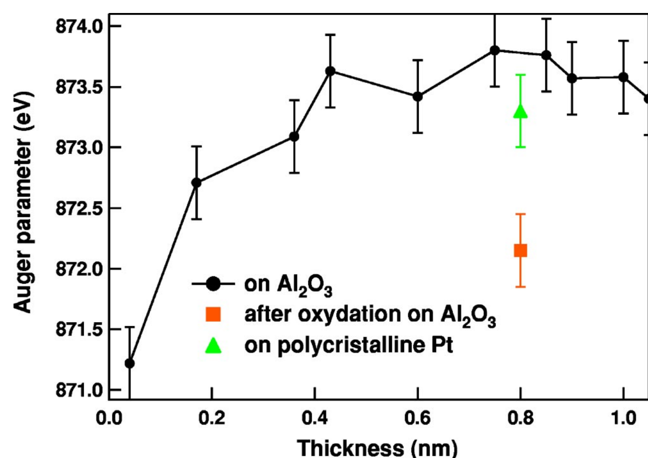

FIG. 4. (Color online) Evolution of the titanium Auger parameter with the mean deposited Ti thickness during the Ti/alumina growth. The two extra points correspond to complementary measurements made on a Ti-covered polycrystalline platinum foil and on a fully oxidized titanium film on alumina (see the text).

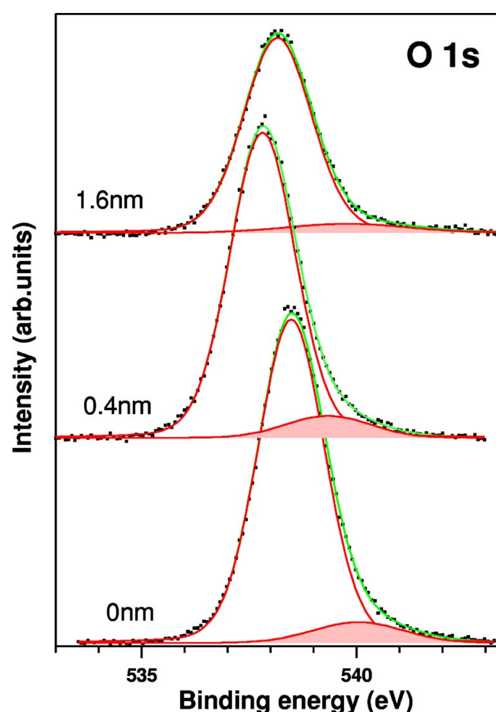

FIG. 5. (Color online) Evolution of the O 1*s* core level upon deposition of silver on alumina. The equivalent thickness is given in the figure.

other words, that there is no differential charging, the BE of the levels associated to alumina can also be taken as references once they have been calibrated with respect to the Ti metal. So doing, Al 2*s* (Ref. 50) and O 1*s* (Fig. 2) levels of the alumina substrate show up at 119.6 ± 0.2 eV and 531.3 ± 0.2 eV, respectively. (In the absence of a defined Fermi level in the band gap of alumina, these values only characterize the present Ti/alumina system. They cannot be used as general spectroscopic characteristics of the bare alumina substrate.)

2. The Ti-OH *reaction*

A straightforward explanation for the interfacial Ti oxidation is the Ti-OH reaction. However, the observed O 1*s* shift might have other origins, such as screening by the metal overlayer, atomic exchange between Ti and Al,[18] metal-oxide bonding[6] and, finally, a reduction of alumina by Ti. First of all, because it is associated to surface species, the O 1*s* shift could be due to screening by the Ti film. To elucidate this point, the present behavior was compared to that of silver which is hardly expected to undergo charge transfer.[6,19] Indeed, the absence of perturbation of the +1.5 eV O 1*s* component (Fig. 5) by the Ag film demonstrates that the surface OH are chemically inert with respect to silver and discards screening as a possible origin of the O 1*s* shift at the Ti/alumina interface. An other possibility is an Ti/Al atomic exchange.[18] Since the Al 2*s* spectrum does not show any new feature at the beginning of Al deposition (Fig. 4 of Ref. 50), the Ti-Al exchange would suggest that Al embedded in Ti corresponds to a Al 2*s* shift similar to that of oxidized Al (−2.6 eV, see below) with respect to bulk Al metal. This being unlikely, the assumption of Ti-Al exchange is ruled out. The formation of Ti-alumina bonds can be then foreseen. Except at submonolayer coverage,[6] transition metal-oxide bonds are predicted to be mostly covalent.[1,31,57–60] The electronic levels of the Ti-covered alumina should then undergo marginal change. Moreover, even when the metal-oxide bonding is partly ionic, the charge of the surface oxygen is predicted to be hardly perturbed by the metal adlayer.[8,20] In this respect, the Ti-induced −2.8 eV shift appears quite strong. Taking as a reference the O 1*s* shift associated to the different ionic oxygen species,[61] it would correspond to a charge transfer of ~0.5 electron, a value hardly acceptable in view of the dominant covalency of the Ti-alumina bond. Thus, the occurrence of Ti-alumina bonds to explain the O 1*s* shift can be rejected. Finally, scrutinizing the Al 2*p* spectra (see Fig. 4 of Ref. 50) does not reveal any change on its lower BE side, where reduced species would show up. Since the limit for the detection of Al/alumina is 2×10^{14} atoms cm^{-2} (as determined by comparison with spectra shown below), i.e., one order of magnitude lower than a full monolayer, it is concluded that the Ti oxidation is not accompanied by a reduction of alumina. [In a similar way, iron was reported to be oxidized into Fe^{2+} at the interface Fe/α-$Al_2O_3(0001)$ while the aluminium core level remained unperturbed,[62] although the explanation given in that case differs from ours.]

The O 1*s* and Ti 2*p* shifts thus originate from the Ti-OH reaction. The +1.5 eV O 1*s* component arises from both the surface OH and an oxygen species that resists annealing in UHV at high temperature. Because of the defined +1.5 eV and −2.8 eV shifts, the latter is also attributed to surface OH, in agreement with Niu *et al.*[14,15,52] This reconciles seemingly contradictory observations of a strong O 1*s* shift upon Ti oxidation and of the absence of Al 2*s* shift. The +1.5 eV and −2.8 eV shifts are hereafter labeled O 1*s*(OH) and O 1*s*(TiO_x), respectively. The assignment of O 1*s*(TiO_x) is supported by the oxidation of a 0.9 nm thick Ti layer that was exposed at 300 K to 10^{-3} Pa of oxygen and then an-

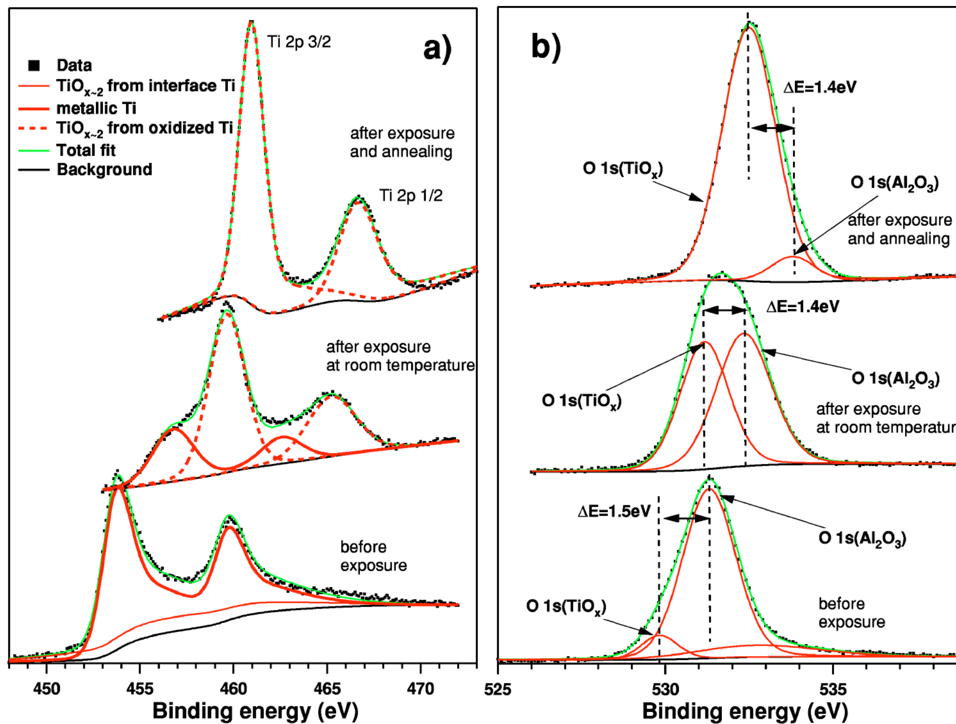

FIG. 6. (Color online) Evolution of the line shapes of (a) Ti $2p$ and (b) O $1s$ core levels during oxidation of a 0.9 nm titanium layer on α-$Al_2O_3(0001)$. The oxidation is performed by exposure for several minutes to an equivalent molecular oxygen pressure of 10^{-3} Pa either at room temperature or by annealing the substrate at $T \simeq 800$ K.

nealed at $T \simeq 800$ K to form a TiO_2 film[63] (Fig. 6) which stoichiometry was checked by photoemission. The O $1s$ shift (Fig. 3) and Auger parameter (Fig. 4) recorded on this sample compare reasonably with those recorded on the first oxidized Ti/alumina layer. An important conclusion is that the persistence of residual OH groups even after annealing under vacuum implies that the clean (Al-terminated) α-$Al_2O_3(0001)$ does not exist in experimental environments. [The coverage of the residual OH groups can be estimated to $3.\pm 1.5 \times 10^{14}$ OH cm^{-2} by means of the O $1s$ (OH) peak area after annealing in vacuum.[50]] Moreover, the structure of the actual surface is not known. The structure determined by surface x-ray diffraction[64] does not involve surface OH groups although they do exist. Clearly, experimental evidence to discuss the various models that were proposed about the hydroxylated alumina surfaces[6,24,65–68] are lacking.

At the early beginning of the growth of the Ti film, a unique oxidation state $Ti^{(n+)}$ is observed [Fig. 2(a), 0.03 nm Ti]. At slightly higher coverage, a second oxidation state is seen [Fig. 2(a), 0.07 nm Ti]. It is only above 0.2 nm Ti, that a Ti $2p$ level corresponding to Ti metal can be identified (Fig. 2). The Ti $2p$ components related to oxidation states are recorded in the energy ranges 458–459 eV and 455–456.5 eV [Fig. 3(a)]. By comparison with tabulated values, they are attributed to $Ti^{(4+)}$ [458.8 eV (Ref. 56)] and $Ti^{(2+)}$ [455 eV (Ref. 56)], respectively, in agreement with the low value of the Auger parameter at the beginning of the growth[56] (see Fig. 4). Finally, the validity of the reference level that allows the assignment of the Ti $2p$ shifted components to oxidized Ti is fully confirmed by the constant observation of these shifts in the presence of the growing metallic Ti film and independently of the Ti thickness (up to 0.6 nm to 0.9 nm, Fig. 3 and Fig. 2), as possible charging effects are expected to vanish. This clearly demontrates the validity of the above assumptions of constant lineup and of the absence of differential charging at the growing interface.

The decomposition of OH groups at the contact with metallic Ti could formally result from the following chemical reaction:[17]

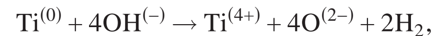

$$Ti^{(0)} + 4OH^{(-)} \rightarrow Ti^{(4+)} + 4O^{(2-)} + 2H_2,$$

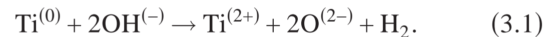

$$Ti^{(0)} + 2OH^{(-)} \rightarrow Ti^{(2+)} + 2O^{(2-)} + H_2. \qquad (3.1)$$

At 0.2 nm Ti, 80% of the oxidized Ti is formed (100% of Ti^{4+} and 60% of Ti^{2+}, see Fig. 7). The good spreading of Ti/alumina at this stage was already noticed.[29] It compares to that observed for Co/α-$Al_2O_3(0001)$.[17] The total OH coverage of the hydroxylated surface corresponding to spectra shown in Fig. 1 of Ref. 50 and Fig. 2 is 0.9×10^{15} OH cm^{-2}, as determined by the area of O $1s$ (OH) (Ref. 21 and 51) (Fig. 7). This is much lower than the estimate of 1.7×10^{15} OH cm^{-2} which is derived from the Ti^{2+} and Ti^{4+} peak areas (Fig. 7). However, a careful examination of the O $1s$ line does not reveal any change above 0.6 nm Ti, which discards any Ti oxidation by the residual gases. Therefore, the discrepancy between OH coverage and the oxidized Ti amount is suggested to arise from a under-stoichiometry of the Ti oxides with respect to that would be expected by considering the formal charges Ti^{4+} and Ti^{2+}.

3. Dominant ionic bonding at the aluminium/alumina interface

The Al $2s$ and O $1s$ spectra recorded during the growth of the Al/α-$Al_2O_3(0001)$ are shown in Fig. 7. As in the case of Ti/alumina, the O $1s$ (OH) feature shifts as a whole [Fig. 8(b)]. The Al-OH reaction produces an interfacial oxide AlO_x, since the Al $2s$ level corresponding to metallic Al only shows up above 0.2 nm Al [Fig. 8(a)]. It then peaks at -2.8 eV with respect to the alumina Al $2s$ level, a value compatible with the Al^0/Al^{3+} shift.[69] Bulk plasmon energy

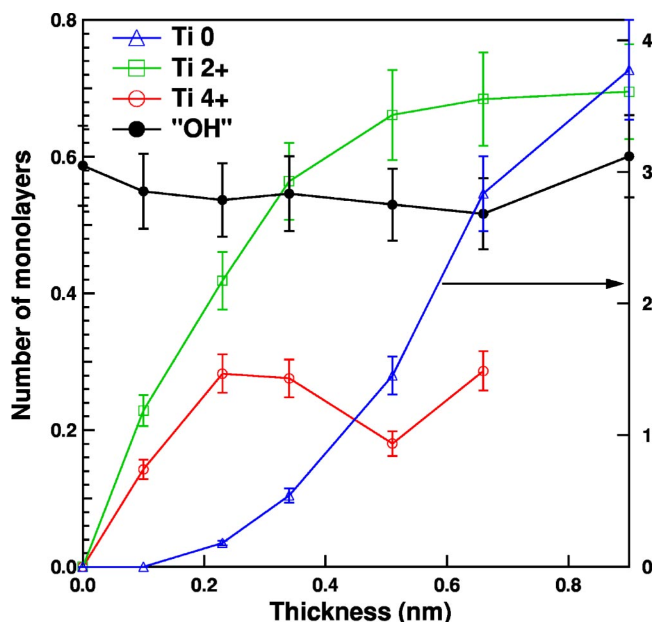

FIG. 7. (Color online) Evolution of the area of the various Ti $2p$ components and of the O $1s$(OH) during the Ti/alumina growth (the Ti thickness is given in the figure). The monolayer is defined by the oxygen plane of the corindon structure. These amounts have been obtained from the peak integrated intensities normalized by the O $1s$ substrate line without accounting of the attenuation of the signal in the titanium overlayer.

losses of 15 eV [Fig. 8(c)] provide an other evidence for the metallicity of the Al film. The island growth (see below) and the lack of percolation in the film explains the reminiscence of charging effect even for 1 nm Al. In fact, below 0.2 nm, neither the O $1s(AlO_x)$ peak nor the Al $2s$ level associated to the growing film can be distinguished from the O $1s$ and Al $2s$ bulk alumina levels (Fig. 8). This suggests that AlO_x does not differ much from the alumina substrate, in agreement with calculations predicting that ionic Al-O bonds dominate the Al/α-Al_2O_3(0001) interface for both Al- and O-terminated alumina[8,20] and that the interface atoms are in positions corresponding to the alumina lattice.[8,16] Note that, below 0.2 nm, the growing Al/alumina film always gives rise to a (1×1) LEED pattern and never shows any extra spot that could be compared to the reconstructions[41,70] which are obtained by annealing the α-Al_2O_3(0001) surface in vacuum. Above 0.2 nm, charging effects due to growing clusters prevents LEED observations. These findings are in agreement with those of other groups.[36,37]

4. Ti/alumina and Al/alumina epitaxies

On Ti/alumina films, the Ti $2p$ intensity peaks at angles (0°, 31.5°, and 35.3°) that are characteristic of forward scattering from an hexagonal compact lattice observed within the [0001] direction [Fig. 9(b)]. In addition, the angular dependence recorded on the O $1s$ peak [Fig. 9(b)] reveals some matching between the alumina and the Ti arrays. This finding is consistent with the known Ti/alumina epitaxy (0001)Ti$\|$(0001)Al_2O_3 and $[1\bar{1}00]$Ti$\|[2\bar{1}\bar{1}0]Al_2O_3$, as determined by transmission electron microscopy (TEM)[32] and high energy electron diffraction (RHEED).[32,54,55,71] Nevertheless, the broadness of these profiles indicates a somewhat desordered adlayer. Instead, the Al $2s$ intensity profile recorded from Al/alumina films shows sharp structures at 0°, 19°, 35°, and 55°. In agreement with the general consensus about the Al/α-Al_2O_3(0001) interface,[8,36,37,72] these charac-

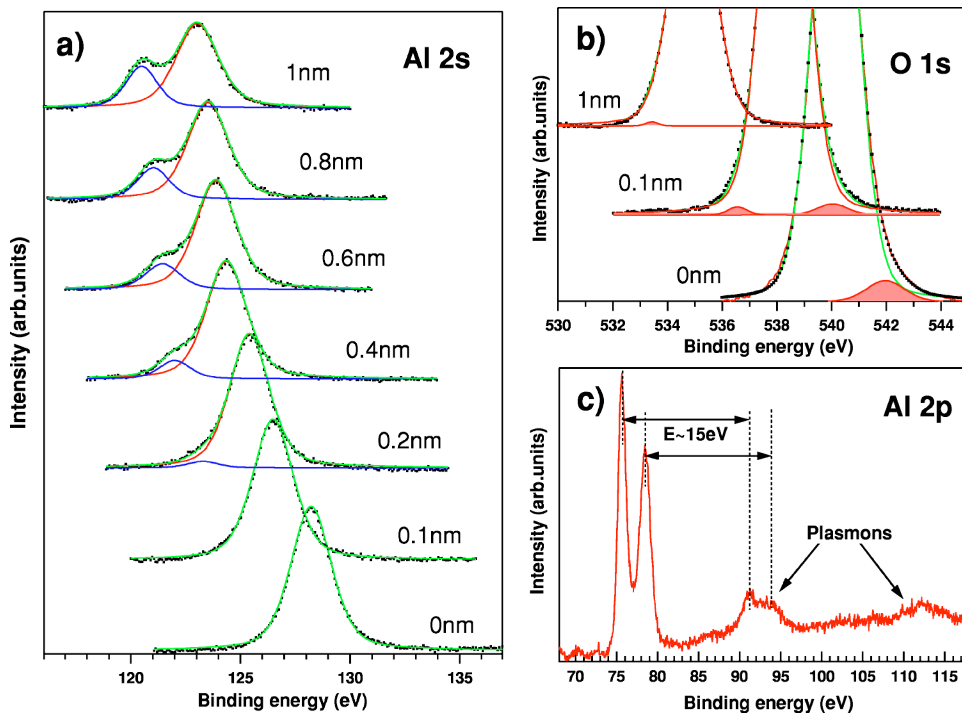

FIG. 8. (Color online) XPS spectra of the (a) Al $2s$, (b) O $1s$, and (c) Al $2p$ core levels recorded during the deposition of aluminium on α-Al_2O_3(0001) at room temperature. Also shown are the plasmon loss structures separated by 15 eV from the core levels.

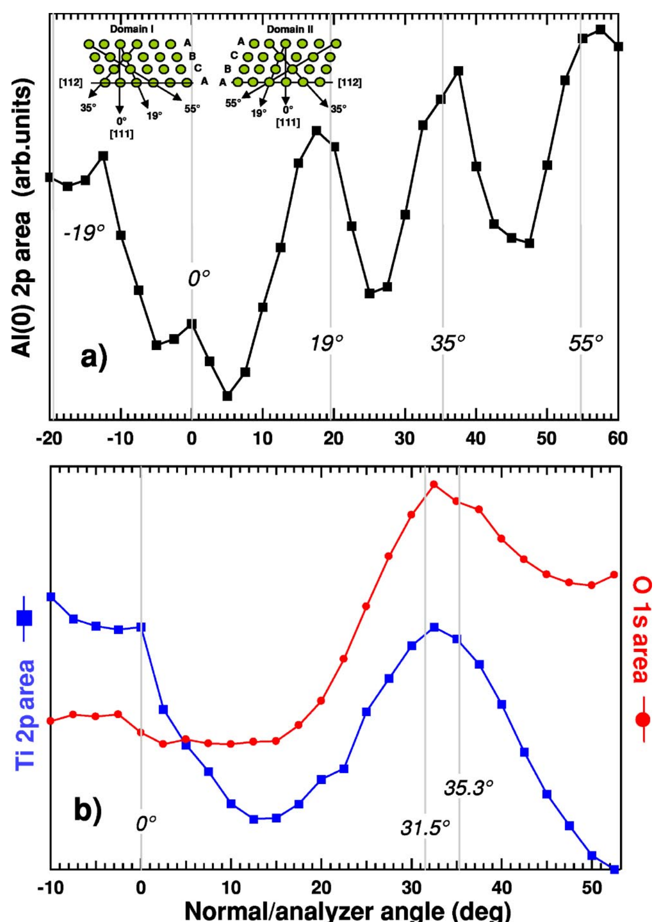

FIG. 9. (Color online) Photoemission integrated intensities modulation versus collection angle (forward scattering) for (a) Al $2p$ and (b) Ti $2p$ core levels acquired at the end of the growth of Al(3 nm) and Ti(1.4 nm) films on α-Al_2O_3(0001).

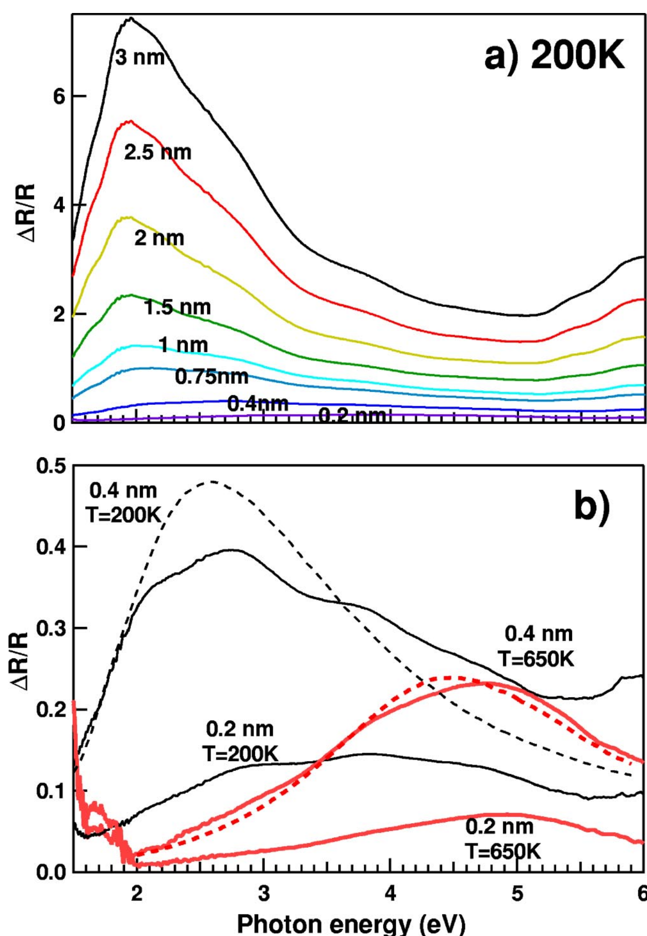

FIG. 10. (Color online) SDR spectra collected during the deposition of aluminium on α-Al_2O_3(0001) (the thickness is given in the figure) at (a) 200 K. (b) Early beginning of the growth, spectra corresponding to thicknesses of 0.2 nm and 0.4 nm for Al/alumina films grown at 200 K and 600 K. Also displayed are the associated fits (dashed lines) with particles modeled by truncated spheroidal shapes.

terize a strong forward scattering of an ordered cubic-face-centered arrangement observed in a [111] direction [Fig. 9(a)], with two epitaxial variants at 180° associated to *ABC* or *BCA* stackings.[73]

B. The wetting of hydroxylated α-Al_2O_3(0001) by aluminium and titanium

The above data demonstrate that the M-O bond under study are governed by metal-OH reactions. When deposited on hydroxylated α-Al_2O_3(0001), the first ML of Ti and Al react with surface OH groups to produce an interfacial oxide layer. In similar cases, at the Rh/ and Cu/alumina interfaces,[13,15,16,52] the presence of hydroxyl groups at the surface of the oxide was shown to enhance the bonding of the metal layer. OH groups have even been stressed to promote a laminar growth of Co/alumina.[17] Now, to know whether the interfacial oxide layer improves the wetting of a further deposited metallic film, the behavior of the growing adlayer was studied *in situ* by SDR spectroscopy.

1. The Al/α-Al_2O_3(0001) *interface*

SDR spectra recorded during the growth of Al/α-Al_2O_3(0001) at 200 K [Fig. 10(a)]. The faint but real broad structure appearing in the near ultraviolet at the beginning of the growth of the metallic Al film (0.2 nm) (Fig. 10) proves the existence of three-dimensional (3D) particles since the polarization of a thin continuous film by a UV-visible electromagnetic field does not occur for film thickness lower than 0.6 to 0.7 nm.[74] This even discards a Stranski-Krastanov growth mode which supposes at least one continuous atomic layer. Consistently, charging effects are still observed on the 1 nm thick Al film and the AFM image of a 3 nm thick Al/alumina film deposited at 600 K shows 3D clusters on the way to coalesce [Fig. 11(a)]. Because the Al bulk plasmon is located around 15 eV and the Frölich mode of an isolated aluminium sphere is around 9 eV, a resonance below 6 eV characterizes particles with a high aspect ratio. Notice, however, how the growth crucially depends on the temperature. Indeed, SDR spectra recorded during the growth of Al/α-Al_2O_3(0001) at 200 K are shown in [Fig. 10(a)] and 600 K (Ref. 50) are seen to strongly differ [Fig. 10(b)]. They can be assigned to truncated spheroids with aspect ratios of 7.5 and 4.2, respectively, corresponding

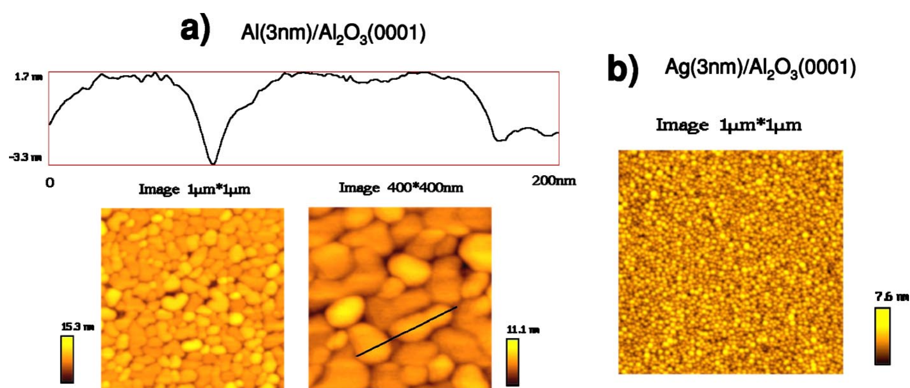

FIG. 11. (Color online) *Ex situ* atomic force microscopy images of metal depositions on α-$Al_2O_3(0001)$: (a) Al(3 nm), (b) Ag(3 nm). The profile along the indicated line for aluminium deposition shows flat top islands.

to contact angles of 30° and 51°. (Al clusters are best modeled as spheroids,[28,29] but contact angles are easier to define using truncated spheres. The same will be done with Ti clusters.) For the same system, the contact angle determined by sessile drop measurements is 86°,[35] in agreement with adhesion values of 950 mJ m^{-2},[75] 955 mJ m^{-2},[5] 1070 mJ m^{-2},[76] and 1130 mJ m^{-2} (scaled to 0 K)[77] that lead to angles of ~90°. The discrepancy between the value collected at 600 K (51°, close to equilibrium, with a supersation of 10) and these values, might stem from either the method of determination or kinetic effects. Nevertheless, a qualitative agreement can be emphasized, in that all measurements including ours, unambiguously indicate a 3D growth mode.

The Al/α-$Al_2O_3(0001)$ interface has been modeled on both the Al-terminated (Al-Al_2O_3) and the O-terminated (O-Al_2O_3) surfaces.[8] On Al-Al_2O_3, one third of the octahedral sites of oxygen is occupied by Al surface atoms, which represent one-half of a bulk Al (0001) layer. O-Al_2O_3 is simply obtained by removing the Al surface atoms, leaving the surface with three dangling bonds for each Al atom which is removed.[8] Al is expected to partially wet Al-Al_2O_3, with W_{adh} close to γ_{Al}.[7,8,19,20] Instead, for Al/Al_2O_3, theory predicts a perfect wetting with strong adhesion energy (10 J m^{-2},[7,8,20] which is 10 times higher than the Al/Al-Al_2O_3 adhesion and five times higher than the critical value for perfect wetting). In turn, the change in ionic bonding at the interface is suggested to be responsible for the creation of a series of voids in the electron density between the ionized Al and the remainder of the Al slab. These regions of low density should produce a cleavage at the Me-Me/Me-O-Al interface[8] similar to that expected for Nb/O-Al_2O_3.[60] Because of its capability to oxidize the first metallic adlayer (due to its OH coverage), the α-$Al_2O_3(0001)$ compares to O-Al_2O_3. This leads us to assume (i) that the hydrogen adatom actually stabilizes the O-Al_2O_3 surface and (ii) that the adhesion energy of the oxidized Al formed by the Al-OH reaction is of the order of that of Al/O-Al_2O_3. However, optics and AFM demonstrate that the metallic Al film does not perfectly wet the intermediate Al oxide layer, a behavior in agreement with the predicted Al-Al/Al-O-Al cleavage at the Al/O-Al_2O_3 interface.[8]

2. The partial wetting of titanium on hydroxylated alumina

As an early transition metal, Ti exhibits a bulk plasmon resonance strongly attenuated by interband transitions around 2 and 4 eV.[78] At the beginning of the growth of the film at 300 K, corresponding SDR features are visible at 0.4 nm Ti (see Fig. 13 of Ref. 29). As in the case of Al/alumina, the appearance of resonances at low coverage proves that the Ti film is in the form of 3D clusters even at a total coverage of 0.4 nm (i.e., 0.2 nm of oxide and 0.2 nm of metal, see above). The experimental data were previously shown to be compatible with the formation of flat clusters of aspect ratio close to 8 (see Fig. 14 of Ref. 29), in agreement with the presence of sharp RHEED strikes during growth.[54,55,71] This 3D growth mode is qualitatively consistent with the thermodynamic data, although the present observation defines a much smaller contact angle than the sessile drop value of 78° (Refs. 5 and 12) which would lead to an aspect ratio of 3. The 2D-like growth mode (3D in nature) likely arises from the high supersaturation (~60) which reigns during the growth of the refractory Ti film. Under these conditions, a high nucleation rate and a limited mobility should lead to the formation of a high density of 3D clusters which are expected to merge into a continuum layer as the coverage increases,[79] a view supported by the AFM image in which the steps of the clean alumina surface are still visible.[27] Indeed, in the absence of optical SDR data, this observation could misleadingly suggest a 2D growth mode. Ti behaves in a similar manner as Al. The very first layer oxidized via the Ti-OH reaction likely forms strong bonds with alumina, but, because of the weakening of the Ti-Ti backbonds, the metal layer does not (perfectly) wet this intermediate oxidized layer. In agreement with other predictions related to metal/Al_2O_3(O) systems,[8,60] the cleavage is expected to occur at the Ti-Ti/Ti-O-Al interface. Another example in the same spirit is given by the Ti-promoted adhesion of Ag/alumina.

C. The enhancement of the wetting of silver/alumina by metallic titanium

In microelectronics devices, titanium helps wetting silica or alumina by copper[30,32] and early transition metal films are

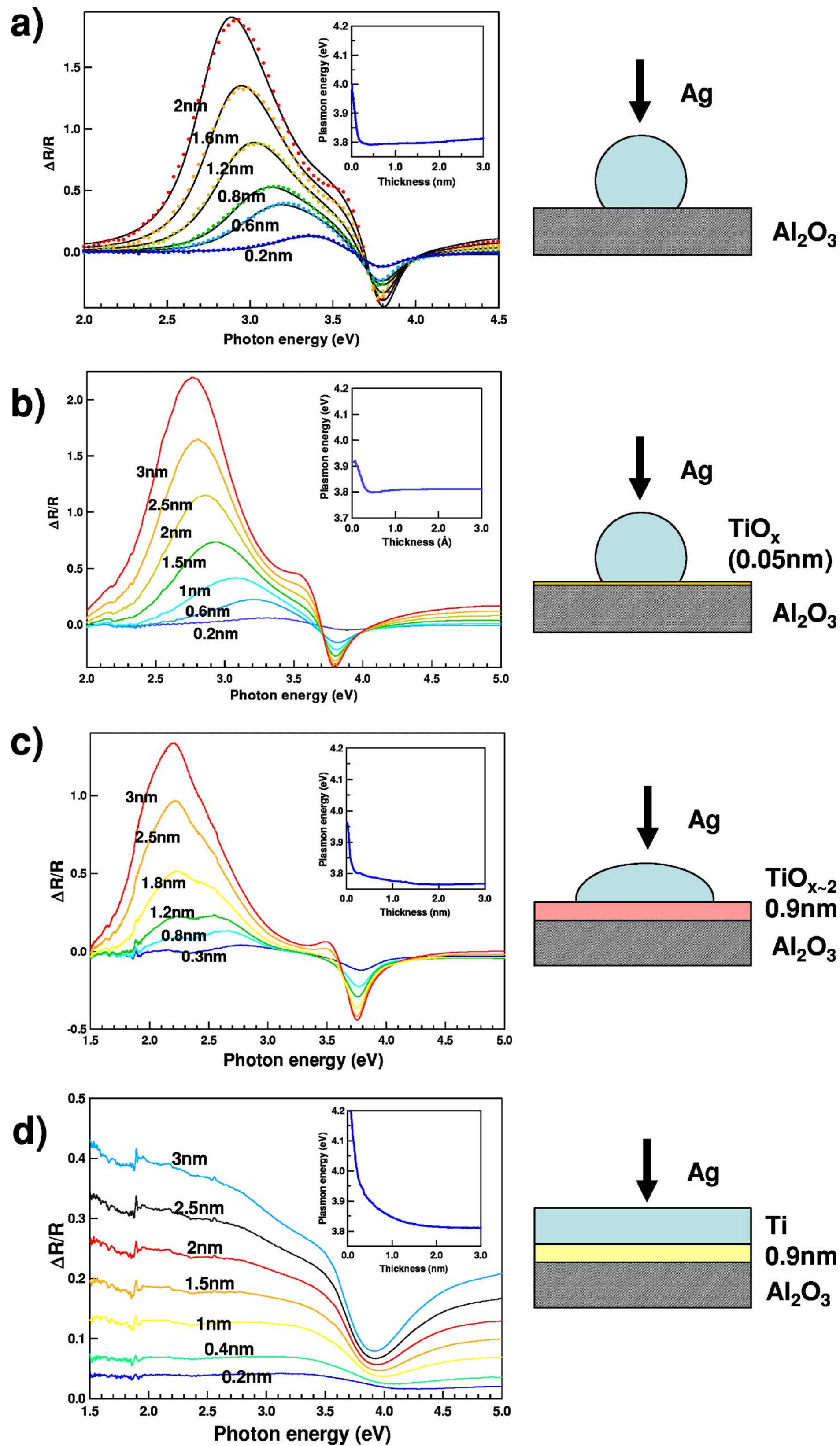

FIG. 12. (Color online) SDR spectra of (a) Ag/alumina, (b) Ag/0.1 nm Ti/alumina, (c) Ag/1.6 nm TiO_x/alumina and (d) Ag/0.9 nm Ti/alumina stackings. Shifts in energy of the high energy resonance observed in *p* polarization with silver equivalent thickness is shown in the insets. Calculated SDR spectra for truncated spheres are given for the Ag/alumina growth [full lines in (a)]. The spectra of (d) have been acquired in *s* polarization. The schematic representations of the silver film shown on the right-hand side are derived from the SDR spectra (see the text).

used as buffers in steel industry for bonding protective ceramic coatings.[30,31] Of relevance to the present study, titanium is often used as a promoter of adhesion between alumina and metallic media.[25,27,30–33] Indeed, a metallic Ti layer has been shown to enhance the wetting of alumina by silver.[29] However, the prediction that a Ti monolayer deposited on the alumina could glue the silver film through an electronic depletion at the interface[30,31] has never been checked, although the above demonstrated oxidation of the first Ti layer at the contact with the hydroxylated alumina resembles the predicted Ti/spinel interface.[30,31] In what follows, the thickness-dependent (chemistry-dependent) effect of a Ti buffer on the Ag/alumina wetting is examined.

The optical SDR technique is expected to be very sensitive to any change in wetting since the polarizability of the particles, which drives their optical response, depends mainly on their aspect ratio.[29] The SDR spectra collected *in situ* during the Ag/alumina growth at 300 K show two resonances [Fig. 12(a)] associated to optical absorptions known as the Mie resonances. They arise from a polarization process of the electronic gas by the components of the *p*-polarized electric field which are either parallel (positive low energy peak in SDR) or perpendicular (negative high energy peak) to the surface.[29,44] The occurrence of resonances even at very low coverage is indicative of 3D growth,[74] in agreement with the AFM images [Fig. 11(b)]. Consistently, the position in energy of the high energy resonance (<3.70 eV) below the bulk plasmon resonance (3.76 eV) demonstrates the formation of particles with contact angle much higher than 90° (low aspect ratio).[27,80] The SDR spectra can be fitted by representing particles are by truncated spheres[44–46] [Fig. 12(a)] whose contact angle is 127°, very close to the sessile drop value of 127–131°.[5,12] Finally, the Ag/alumina sticking coefficient at 300 K which is derived by comparison of the SDR estimate of the thickness with the quartz value is close to one.

Ag films have been then deposited on Ti-covered alumina at various thickness. An important finding is that the 0.05 nm thick Ti film does not much affect the Ag growth with respect to the bare alumina [Fig. 12(b) compared to Fig. 12(a)], in apparent contradiction with the above prediction of Ti gluing the silver. The modest redshift of the low energy resonance indicates a small increase in the aspect ratio; the fit of these spectra leads to a contact angle $\sim 110°$. In contrast, a strong change occurs on alumina precovered by a 0.9 nm Ti film [Fig. 12(d)], i.e., when Ti is metallic.[29] The energy position of the low energy SDR resonance is strongly redshifted as the aspect ratio increases. For very high values of that parameter (or 2D growth), SDR spectra only show a progressive increase in intensity towards the red, as in Fig. 12(d). A similar indication is given by the position in energy of the high energy resonance [see inset of Fig. 12(d)], i.e., 4.2 eV up to an average thickness of 0.2 nm.[74] Then, this high energy peak shifts continuously towards the surface plasmon frequency of a thin continuous layer, i.e., 3.8 eV, where 3D clusters would produce resonances below this value as in Fig. 12(a)–12(c). The difference in surface energy of Ti and Ag (Ref. 12) could explain the observed 2D growth of silver on a metallic Ti layer. To check that the metallicity of the Ti layer is a necessary condition to promote the Ag wetting, a 0.9 nm thick Ti layer was oxidized prior to depositing Ag (Fig. 6).[63] The subsequent Ag growth [Fig. 12(c)] resembles that obtained directly on $TiO_2(110)$ surface.[81] It is clearly 3D. However, according to the position of the low energy SDR resonance (2.2 eV), the Ag wetting is improved with respect to bare alumina, as expected from the smaller band gap of titanium oxide.[5,11]

Kötlmeier and Elsässer[30,31] have performed *ab initio* theoretical calculations on the Ti and Al buffer effects for Ag/(Mg, Al, O) spinels. They have chosen metal/spinel assemblies with low lattice mismatch (metal=aluminium, titanium and silver) to minimize elastoplastic relaxation effects. They have considered the role of Ti as a promoter of Ag adhesion on the spinel. The Ti-spinel bond being mostly covalent, empty electronic states of Ti were suggested to act as a glue for the Ag adlayer so that a unique atomic layer of Ti inserted at the interface should promote the Ag/spinel adhesion. In contrast, in the present experiment, a unique atomic adlayer of Ti on alumina hardly improves the wetting by Ag. Clearly, in the calculation of Köstlmeier and Elsässer, a covalent bonding takes place between the Ti interlayer and the spinel surface, but the Ti is not oxidized. Indeed, the oxidation of the Ti buffer layer in contact with the hydroxylated alumina leads to a totally different situation. Instead of being glued to the alumina by an electron-depleted metallic Ti adlayer, the Ag film is deposited on another oxide, the Ti oxide which results from the Ti-OH chemical reaction. In fact, it is the surface hydroxylation of alumina groups that causes the glue mechanism not to hold.

IV. CONCLUSION

A residual hydroxylation is shown to always remain on the α-$Al_2O_3(0001)$ surface in experimental conditions, even after annealing under ultrahigh vacuum. Therefore, there exist both reversibly and irreversibly adsorbed OHs. It was chosen herein to study the growth of metallic films on a hydroxylated alumina surface. By means of the analysis by photoemission and UV-visible reflectivity, both the growth modes and the interfacial chemistry could be determined *in situ* simultaneously.

At the early beginning of the Al and Ti film growth, surface OH groups react with metals to give rise to an oxidized intermediate layer strictly confined to the interface. Although the structure of the real alumina surface is still not known, the present analysis suggests that the best modeling of the metal/hydroxylated α-$Al_2O_3(0001)$ interface is likely the metal/O-terminated alumina model. The growth mode of the Al and Ti metallic films which are deposited on these intermediate oxidized layers is unambiguously 3D, a behavior which compares with predictions for Al and Nb deposited on O-terminated alumina. This 3D growth mode indicates that the cleavage at the metal/alumina assemblies would preferentially occur at the Me-Me/Me-O-Al interface (Me=Al, Ti). The present findings are consistent with calculations which inferred that the charge transfer due to the strong

metal-oxide bond formed via the metal-OH reaction results in a weakening of the metal-metal backbonds. The same applies when Ti is used as a buffer. The thin oxidized Ti intermediate layer is inefficient to promote the Ag/alumina wetting. However, a strong improvement of the Ag/Ti/alumina wetting is achieved by metallic Ti.

Although it has not been possible to compare hydroxylated alumina to bare alumina that we were unable to obtain, it appears that the presence of hydroxyl groups does not greatly increase the adhesion of metallic films at the surface of alumina.

ACKNOWLEDGEMENTS

The authors are grateful to Jacek Goniakowski (Groupe de Physique des Solides, Paris) for fruitful discussions and acknowledge the invaluable technical support of Pascal Naël from Saint-Gobain Recherche (Aubervilliers).

*Electronic address: lazzari@gps.jussieu.fr
†Electronic address: jupille@jussieu.fr
[1] K. H. Johnson and S. V. Pepper, J. Appl. Phys. **53**, 6634 (1982).
[2] T. C. Campbell, Surf. Sci. Rep. **27**, 1 (1997).
[3] P. Alemany, R. S. Boorse, J. Burlitch, and R. Hoffman, J. Phys. Chem. **97**, 8464 (1993).
[4] J. Goniakowski, Phys. Rev. B **59**, 11047 (1999).
[5] D. Chatain, L. Coudurier, and N. Eustathjopoulos, Rev. Phys. Appl. **23**, 1055 (1988).
[6] C. Verdozzi, D. R. Jennison, P. A. Schultz, and M. P. Sears, Phys. Rev. Lett. **82**, 799 (1999).
[7] W. Zhang and J. Smith, Phys. Rev. B **61**, 16 883 (2000).
[8] D. Siegel, L. Victor, and J. Adams, Phys. Rev. B **65**, 085415 (2002).
[9] A. Stoneham, Appl. Surf. Sci. **14**, 249 (1983).
[10] Y. Naidich, Prog. Surf. Membr. Sci. **14**, 353 (1981).
[11] F. Didier and J. Jupille, J. Adhes. **58**, 253 (1996).
[12] D. Chatain, L. Coudurier, and N. Eustathopoulos, J. Chem. Phys. **83**, 561 (1986).
[13] J. Libuda, M. Frank, A. Sandell, S. Andersson, P. A. Brühwiler, M. Baümer, N. Mårtenson, and H. J. Freund, Surf. Sci. **384**, 106 (1997).
[14] D. R. Jennison and A. Bogicevic, Faraday Discuss. **114**, 45 (1999).
[15] A. Kelber, C. Niu, K. Shepherd, D. R. Jennison, and A. Bogicevic, Surf. Sci. **446**, 76 (2000).
[16] X. Wang, J. Smith, and M. Scheffler, Phys. Rev. B **66**, 073411 (2002).
[17] S. Chambers, T. Droubay, D. Jennison, and T. Mattsson, Science **297**, 827 (2002).
[18] C. Verdozzi, P. Schultz, R. Wu, A. Edwards, and N. Kioussis, Phys. Rev. B **66**, 125408 (2002).
[19] J. Smith and W. Zhang, Acta Mater. **48**, 4395 (2000).
[20] I. Batyrev and L. Kleinman, Phys. Rev. B **64**, 033410 (2001).
[21] V. Coustet and J. Jupille, Surf. Sci. **307–309**, 1161 (1994).
[22] J. W. Elam, J. Phys. Chem. **102**, 7008 (1998).
[23] P. J. Eng, T. P. Trianor, G. E. Brown, G. A. Waychunas, M. Newville, S. R. Sutton, and M. L. Rivers, Science **288**, 1029 (2000).
[24] K. Hass, W. Schneider, A. Curioni, and W. Andreoni, Science **282**, 265 (1998).
[25] A. Evans, J. Hutchison, and Y. Wei, Acta Mater. **47**, 4093 (1999).
[26] R. Lazzari, J. Jupille, and Y. Borensztein, Appl. Surf. Sci. **142**, 451 (1999).
[27] R. Lazzari and J. Jupille, Surf. Sci. **482–485**, 823 (2001).
[28] I. Simonsen, R. Lazzari, J. Jupille, and S. Roux, Phys. Rev. B **61**, 7722 (2000).
[29] R. Lazzari, I. Simonsen, D. Bedeaux, J. Vlieger, and J. Jupille, Eur. Phys. J. B **24**, 267 (2001).
[30] S. Köstlmeier and C. Elsässer, J. Phys.: Condens. Matter **12**, 1290 (2000).
[31] S. Köstlmeier and C. Elsässer, Interface Sci. **8**, 41 (2000).
[32] G. Dehm, C. Scheu, M. Rühle, and R. Raj, Acta Mater. **46**, 759 (1998).
[33] G. Kästle, H. Boyen, B. Koslowski, A. Plettl, F. Weigl, and P. Ziemann, Surf. Sci. **498**, 168 (2002).
[34] Y. Zhukovskii, E. Kotomina, B. Herschendb, K. Hermanssonb, and P. Jacobs, Surf. Sci. **513**, 343 (2002).
[35] V Laurent, D. Chatain, C. Chatillon, and N. Eustathopoulos, Acta Metall. **36**, 1797 (1988).
[36] M. Vermeersch, R. Sporken, P. Lambin, and R. Caudano, Surf. Sci. **235**, 5 (1990).
[37] M. Vermeersch, F. Malengreau, R. Sporken, and R. Caudano, Surf. Sci. **323**, 175 (1995).
[38] S. Tanuma, C. J. Powell, and D. R. Penn, Surf. Interface Anal. **17**, 911 (1991).
[39] S. Tanuma, C. J. Powell, and D. R. Penn, Surf. Interface Anal. **17**, 927 (1991).
[40] http://www.physik.de/mateck, site for single cristal substrates.
[41] G. Renaud, Surf. Sci. Rep. **32**, 1 (1998).
[42] D. Shirley, Phys. Rev. B **5**, 4709 (1972).
[43] D. Bedeaux and J. Vlieger, *Optical Properties of Surfaces* (Imperial College Press, London, 2001).
[44] R. Lazzari and I. Simonsen, Thin Solid Films **419**, 124 (2002).
[45] R. Lazzari, S. Roux, I. Simonsen, J. Jupille, B. Bedeaux, and V. Vlieger, Phys. Rev. B **65**, 235424 (2002).
[46] R. Lazzari, I. Simonsen, and J. Jupille, Europhys. Lett. **61**, 541 (2003).
[47] R. Lazzari, J. M. Layet, and J. Jupille, Phys. Rev. B **68**, 045428 (2003).
[48] E. D. Palik, *Handbook of Optical Constants of Solids* (Academic, New York, 1985), Vol. 1–2.
[49] C. E. Nelson, J. W. Elam, M. A. Cameron, M. A. Tolbert, and S. M. George, Surf. Sci. **416**, 341 (1998).
[50] R. Lazzari and J. Jupille, Surf. Sci. **507–510**, 683 (2002).
[51] V. Coustet and J. Jupille, Nuovo Cimento Soc. Ital. Fis., D **19D**, 1657 (1997).
[52] C. Niu, K. Shepherd, D. Martini, J. Tong, J. Kelber, D. Jennison, and A. Bogicevic, Surf. Sci. **465**, 163 (2000).
[53] J. Ahn and J. W. Rabalais, Surf. Sci. **388**, 121 (1997).
[54] T. Suzuki, S. Hidhita, K. Oyoshi, and R. Souda, Surf. Sci. **437**, 289 (1999).

[55] E. Søndergård, O. Kerjan, D. Abriou, and J. Jupille, Eur. Phys. J. D **24**, 343 (2003).
[56] C. D. Wagner, W. M. Riggs, L. E. Davis, J. F. Moulder, and G. E. Muilenberg, *Handbook of x-Ray Photoelectron Spectroscopy* (Perkin-Elmer, Eden Prairie, 1979).
[57] U. Schönberger, O. K. Andersen, and M. Methfessel, Acta Metall. **S1**, 1 (1992).
[58] J. G. Li, Compos. Interfaces **1**, 37 (1993).
[59] J. Smith, T. Hong, and D. Srolovitz, Phys. Rev. Lett. **72**, 4021 (1994).
[60] I. Batyrev, A. Alavi, and M. W. Finnis, Faraday Discuss. **114**, 33 (1999).
[61] J. Jupille, P. Dolle, and M. Besançon, Surf. Sci. **260**, 271 (1992).
[62] A. Arranz, V. Pérez-Dieste, and C. Palacio, Surf. Sci. **521**, 77 (2002).
[63] G. Lu, S. Bernasek, and J. Schwartz, Surf. Sci. **458**, 80 (2000).
[64] P. Guénard, G. Renaud, A. Barbier, and M. Gautier-Soyer, Surf. Rev. Lett. **5**, 321 (1998).
[65] M. Causa, R. Dovesi, C. Pisani, and C. Roetti, Surf. Sci. **25**, 119 (1987).
[66] I. Manassidis, J. Am. Ceram. Soc. **77**, 355 (1994).
[67] V. E. Puchin, J. D. Gale, A. L. Shluger, E. A. Kotomin, J. Günster, M. Brause, and V. Kempter, Surf. Sci. **370**, 190 (1997).
[68] X.-G. Wang, A. Chaka, and M. Scheffler, Phys. Rev. Lett. **84**, 3650 (2000).
[69] D. Briggs and M. P. Seah, *Practical Surface Analysis by Auger and X-ray Photoelectron Spectroscopy* (Wiley, New York, 1983).
[70] T. M. French and G. A. Somorjai, J. Phys. Chem. **74**, 2489 (1970).
[71] E. Sondergard, O. Kerjan, C. Barreteau, and J. Jupille, Surf. Sci. **559**, 131 (2004).
[72] D. L. Medlin, K. F. Mac Carty, R. Q. Hwang, S. E. Guthrie, and M. I. Baskes, Thin Solid Films **299**, 110 (1997).
[73] C. Westphal, Surf. Sci. Rep. **50**, 1 (2003).
[74] Y. Borensztein, M. Roy, and R. Alameh, Europhys. Lett. **31**, 311 (1995).
[75] J. J. Brennan and J. A. Pask, J. Am. Ceram. Soc. **51**, 569 (1968).
[76] V. Merlin and N. Eustathopoulos, J. Mater. Sci. **30**, 3619 (1995).
[77] D. M. Lipkin, J. N. Israelachvili, and D. R. Clarke, Philos. Mag. A **76**, 715 (1997).
[78] P. Hadzel and T. Radonń, Vacuum **54**, 125 (1999).
[79] E. Bauer and J. H. van der Merwe, Phys. Rev. B **33**, 3657 (1986).
[80] Y. Borensztein, R. Alameh, and M. Roy, Phys. Rev. B **50**, 1973 (1994).
[81] D. Martin, J. Jupille, and Y. Borensztein, Surf. Sci. **377–379**, 985 (1997).